*High Power Laser Science and Engineering*, (2023), Vol. 11, e64, 16 pages.
doi:10.1017/hpl.2023.53

HIGH POWER LASER SCIENCE AND ENGINEERING

**REVIEW**

# Spectral purity systems applied for laser-produced plasma extreme ultraviolet lithography sources: a review

Nan Lin[1,2,†], Yunyi Chen[1,2,†], Xin Wei[1,2], Wenhe Yang[1,2], and Yuxin Leng[2]

[1] *School of Microelectronics, Shanghai University, Shanghai, China*

[2] *Department of Precision Optics Engineering, Shanghai Institute of Optics and Fine Mechanics, Chinese Academy of Sciences, Shanghai, China*

*(Received 22 March 2023; revised 15 May 2023; accepted 20 June 2023)*

**Abstract**

With the development of high-volume manufacturing for very-large-scale integrated circuits, the purity of the light source in the extreme ultraviolet lithography (EUVL) system needs to fulfil extreme requirements in order to avoid thermal effect, optical distortion and critical dimension errors caused by out-of-band radiations. This paper reviews the key technologies and developments of the spectral purity systems for both a free-standing system and a built-in system integrated with the collector. The main challenges and developing trends are also discussed, with a view towards practical applications for further improvement. Designing and manufacturing spectral purity systems for EUVL is not a single task; rather, it requires systematic considerations for all relevant modules. Moreover, the requirement of spectral purity filters drives the innovation in filtering technologies, optical micromachining and advanced metrology.

**Keywords:** collector mirror; extreme ultraviolet lithography; spectral purity filter

## 1. Introduction

As the main technical support for the development of the semiconductor industry, lithography can be considered as the foundation of the current global information industry. In 1965, Gordon Moore followed the development trend of integrated circuits at the time, and proposed that the number of transistors on the integrated circuit would double about every 18 months, which was the 'Moore's Law'[1] that the industry has been catching up with until now. The revolution of microchip integration puts forward higher demands on lithography technology. According to the Rayleigh criterion[2], the resolution of the lithography process can be improved by reducing the wavelength of the exposure light source or increasing the numerical aperture (NA) of the projection lens:

$$\text{Resolution} = k_1 \frac{\lambda}{NA}, \tag{1}$$

where $\lambda$ is the wavelength of the exposure light source and $k_1$ is the process constant. Currently, the lithography machine with the shortest working wavelength uses 13.5 nm (2% bandwidth) extreme ultraviolet (EUV) light. Generally, there are four ways to produce 13.5 nm EUV radiation: synchrotron radiation source, discharge produced plasma (DPP), laser-assisted discharge plasma (LDP) and laser-produced plasma (LPP). Among them, the synchrotron radiation source[3] can produce high-power EUV radiation with no debris, but the device structure is complex and expensive; the DPP[4] and LDP[5] methods will lead to heat load and corrosion on the electrodes, resulting in damage to the key components; relatively, the light source generated by LPP[6] is much more stable, and the amount of debris is less than with DPP, making it the mainstream of extreme ultraviolet lithography (EUVL) light sources.

The LPP-EUVL light source system mainly consists of three parts, which are the driving laser, Sn droplet targets and the collector, as shown in Figure 1. The light source system is designed in the shape of an ellipse-of-revolution[8], with one focus where Sn droplets are hit and the other far away from the collector, called the intermediate focus (IF). The pre-pulse laser (e.g., 1064 nm neodymium-doped yttrium aluminium garnet (Nd:YAG) laser) firstly gasifies and partially ionizes the droplet target, and then the

Correspondence to: Nan Lin and Yuxin Leng, Department of Precision Optics Engineering, Shanghai Institute of Optics and Fine Mechanics, Chinese Academy of Sciences, Shanghai 201800, China. Email: nanlin@siom.ac.cn (N. Lin); lengyuxin@mail.siom.ac.cn (Y. Leng)

[†]These authors contributed equally to this work.

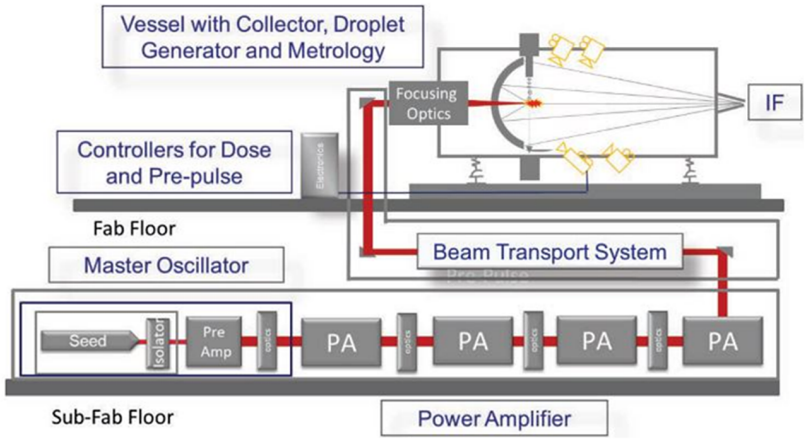


**Figure 1.** Schematic of the LPP-EUVL source system. Reprinted from Ref. [7].

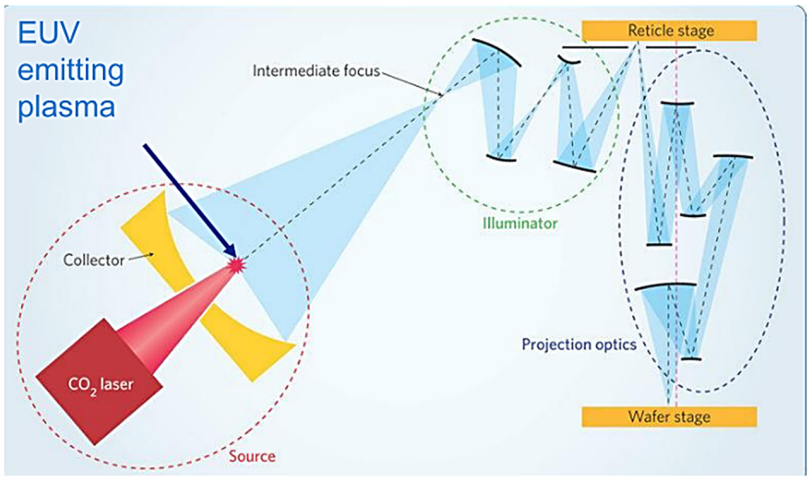


**Figure 2.** Role of the collector in the light source system: the collector collects radiations and reflects them to the IF for subsequent optical path propagation. Reprinted from Ref. [13].

main-pulse laser (e.g., 10.6 μm $CO_2$ laser) completely ionizes the steam group to produce stronger EUV radiation[9]. After that, the collector concentrates and reflects the radiations to the IF for the subsequent optical path propagation[10].

As one of the most important sub-modules, the collector is a multilayer-coated mirror that is in the shape of the graded ellipsoid with 5.5 sr[7,11,12]. With it, the EUV radiation generated can be collected and concentrated to the IF, as shown in Figure 2. In order to satisfy the actual production requirements of EUV radiation with high efficiency, high power and high purity, the collector needs to meet some design specifications[8], such as having a large enough solid collecting angle of 5.5 sr[7,11,12] and a highly reflective multilayer coating, as well as some specific designs to reduce the thermal load of the collector, such as a water-cooling device. However, a collector meeting the above requirements at the same time can also transmit out-of-band (OoB) radiations, that is, radiations other than 13.5 nm (2% band) EUV radiation. Once the OoB radiations are introduced or generated, the light collected and reflected by the collector will no longer be pure, which will not only influence the lithography performance, but also reduce the lifetime of the collector. Thus, it is necessary to design a spectral purity filter (SPF) in the EUVL system to filter out these OoB radiations.

In the past few years, different types of SPFs for EUVL have been designed and manufactured, and some have shown good performance. However, there are no comprehensive reviews or analyses of the research in this field to reflect the latest progress and the existing problems for further study. This paper reviews and discusses the technologies of filtering out OoB radiations in the LPP-EUVL system. Firstly, the influences of OoB radiations on the lithography performance are given. Then, the principles and recent progress of SPFs for EUVL are reviewed and introduced from the aspect of free-standing systems and built-in systems. Major challenges needed to be solved, including the OoB suppression, and manufacturing process as well as different metrologies, etc., are discussed. The technical routes of ASML and

https://doi.org/10.1017/hpl.2023.53 Published online by Cambridge University Press

Gigaphoton, Inc., are specifically discussed. Finally, the future development of SPFs for EUVL is expected in the view of practical applications.

## 2. Out-of-band radiations of the extreme ultraviolet lithography light source

In the light source system, the driven laser hits each Sn droplet target twice to completely ionize it and generate EUV radiation. However, this process not only generates EUV radiation, but also introduces OoB radiations, which are listed in Table 1.

At present, the collector is generally deposited with Mo/Si multilayers to achieve high EUV reflectivity[11]. Figure 3 shows the reflectivity of Mo/Si multilayers to different radiations. It can be found that the EUV reflectivity is close to 70%, while the EUV-OoB reflectivity is so low that it can be neglected. The reflectivity of the ultraviolet (UV)/visible (VIS) spectrum is relevant to EUV radiation, and the reflectivity of infrared (IR) radiation is nearly 100%. If all of these OoB radiations are reflected by the collector and propagate to the subsequent optical path, the performance of the system will be greatly reduced.

For the vacuum ultraviolet (VUV) radiations, they are effectively removed by the background hydrogen, which is originally designed for debris mitigation[16]. The deep ultraviolet (DUV) radiation above 300 nm (i.e., 300–400 nm) in the VIS spectrum has little impact on the lithography performance because the specifically designed photoresistor is generally insensitive to it[17]. In fact, the radiations that have a significant influence on lithography are IR and DUV radiations (130–300 nm). Therefore, most filters in the EUVL system are mainly designed for these two wavelength ranges.

**Table 1.** Radiations in the EUVL light source[14].

| Radiation | Wavelength (nm) |
|---|---|
| (In-band) EUV | 13.5 ± 2% |
| EUV-OoB | 5–70 excluding (in-band) EUV |
| VUV | 70–130 |
| DUV | 130–400 |
| VIS | 400–800 |
| IR | >800 |

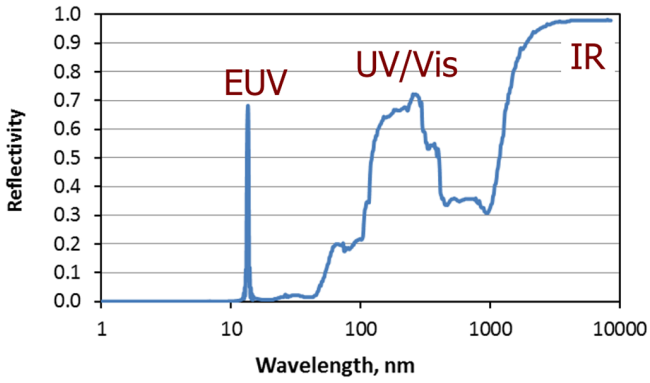


**Figure 3.** Calculated reflectance of the 50-bilayer Mo/Si multilayer coating of 6.9 nm periodicity. Reprinted from Ref. [15].

### 2.1. Infrared radiation

IR radiation comes from the driving lasers (i.e., 10.6 μm $CO_2$ lasers and 1064 nm Nd:YAG lasers) of the LPP-EUVL light source[18]. When generating EUV radiation, the redundant IR radiation of the lasers will also be reflected by the collector and propagated by all the following mirrors, as shown in Figure 2. In the case of the main-pulse $CO_2$ laser with the power of approximately 20 kW, there is approximately 10% of the power (i.e., ~2 kW) that can be collected at the IF[19]. Such high-power radiation will lead to the heating phenomenon[18,20,21] of optics, reticles and wafers, which may cause severe optical distortion and reduce pattern accuracy. For example, since the redundant IR radiation at the IF can be three to five times that of the EUV radiation, the overlay error may exceed eight times the specification[22]. The other problem is that the mirror heating may lead to the mutual diffusion of multilayers, photon-assisted oxidation[23], etc., and these will reduce the lifetime of the optics or even destroy them.

Therefore, the intensity of IR radiation is required to be less than 10% of the EUV radiation at the wafer to prevent damage, which means it needs to be 0.2% or even less of the EUV radiation at the IF[10,12].

### 2.2. Deep ultraviolet radiation

The Sn droplet target hit by the laser will ionize and produce Sn plasma. EUV radiations are generated by the ion transition of $Sn^{7+} - Sn^{10+}$, whereas DUV radiations are mainly generated by $Sn^{1+}$, $Sn^{2+}$ and $Sn^{3+}$[16]. The resistance is very sensitive to the DUV radiation from 150 to 300 nm[17,24], which may lead to unwanted background exposure of the resistance, resulting in the loss of image contrast and critical dimension (CD) bias[16,17]. As depicted in Figure 4, in the exposure system, the DUV reflection at the black border (BB) on a reticle will overexpose the corners and edges of the adjacent field. What is more, in order to prevent the reticle from being polluted, a pellicle is placed on the surface of it. ASML has already invented a pellicle with 90.6% EUV transmissivity[26]. This kind of pellicle has a higher reflectivity of DUV radiation than the BB, so it will have a greater impact on the CD at the corners and edges[14]. However, in practice, wavelengths below 250 nm are usually suppressed due to the reflection of mirrors in the illumination and projection systems[16], so DUV radiation plays a limited role.

https://doi.org/10.1017/hpl.2023.53 Published online by Cambridge University Press

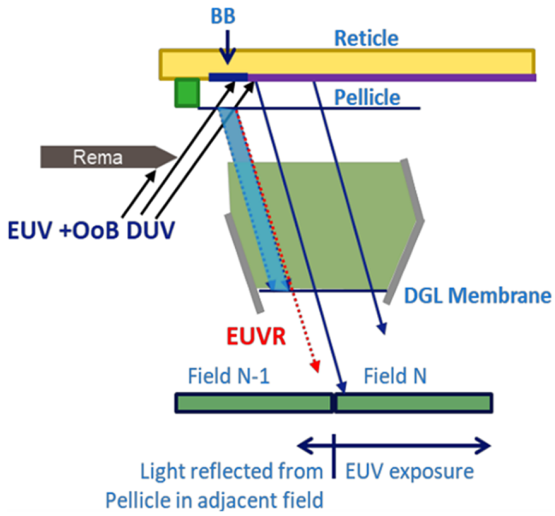


**Figure 4.** The black border's influence on CD errors of the corners and edges of the adjacent field. Reprinted from Ref. [25].

In contrast to IR radiation, the intensity of DUV radiation is related to the characteristics of the droplet, the laser effects and even some unknown elements, such as the optical column reflectivity of DUV radiation and the DUV emission angular dependency of the plasma[16]. Thus, the DUV performance is generally evaluated with dose-to-clear exposure measurement at the wafer level rather than the IF point[16,24]:

$$\frac{\mathrm{DUV}}{\mathrm{EUV}} = \frac{E_0^{\mathrm{ML}}}{E_0^{\mathrm{Cr}}} \cdot 100\%. \tag{2}$$

The ratio of DUV and EUV radiation is determined by the dose-to-clear exposure measurement from both the multilayers and chromium of the reticle. To meet the qualification of EUVL, the value is limited to less than 1% at the wafer[10,12].

## 3. Free-standing spectral purity filters

Since IR and DUV radiations greatly degrade the performance of lithography, it is necessary to filter them out to keep high spectral purity. In the past few years, different kinds of SPFs have been designed and applied in the EUVL system. They can be generally divided into two kinds: free-standing systems and built-in systems. The former refer to filters that serve as independent devices in the source system, including the transmissive SPF and reflective SPF. The latter refer to structures that are integrated with the collector, which will be discussed in Section 4.

### 3.1. Transmissive SPF

A transmissive SPF, which has the structure of periodic multilayers of high and low refractive index materials, is designed to reflect or absorb OoB radiations but transmit EUV radiations. Typical transmissive SPFs include foil filters[27], grid filters[19,22], etc. The transmissive SPF is usually placed before or after the IF, but in some special cases, it is placed between the projection optics and the wafer, as depicted in Figure 5. The transmissive SPF for commercial EUVL needs to meet three primary requirements, namely maintaining high transparency at 13.5 nm ($\hat{A} \pm 2\%$), effectively suppressing OoB radiation and possessing sufficient mechanical strength.

To achieve high EUV transmissivity, a transmissive SPF needs to remain high transparency at 13.5 nm (2%) over a long working time. In contrast to monolayer films, intermetallic membranes have a better performance in IR suppression[28], and thus multilayers composed of different high-transparency materials are studied. Andreev *et al.*[29] compared the performance of filters for EUV radiation, which are constructed with Zr/Si, Nb/Si, Mo/Si or Mo/C multilayers. Bibishkin *et al.*[27] fabricated a Zr/Si filter with the transparency of 76%, and achieved an EUV transmittivity of 78% and suppression ratios from 1000 (UV) to 25 (near IR). Chkhalo *et al.*[28] later found that adding a metallic coating layer and using silicide instead of silicon can relieve the oxidation effect in multilayers. Therefore, they fabricated a $Zr/ZrSi_2$ filter coated with $MoSi_2$ and its transparency only decreased by 4.8%, while the uncoated one decreased by about 10%. Subsequently, they substituted Zr layers with Mo layers and achieved a better performance with an in-band transparency above 70%[30]. Notably, choosing proper materials is a trade-off among EUV transparency, OoB suppression and mechanical strength. Although some materials perform well in transparency, their

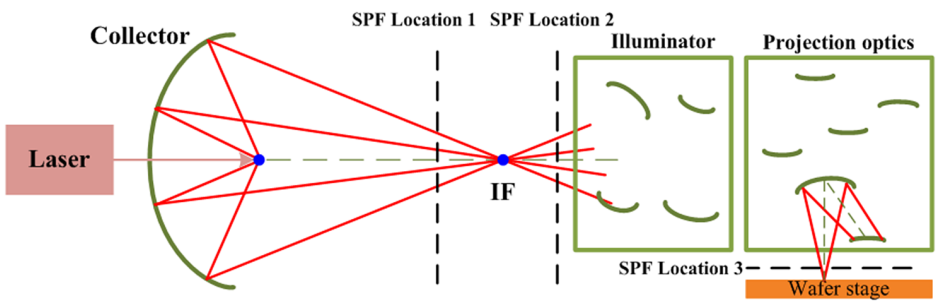


**Figure 5.** EUVL system with possible locations for the transmissive SPF.

https://doi.org/10.1017/hpl.2023.53 Published online by Cambridge University Press

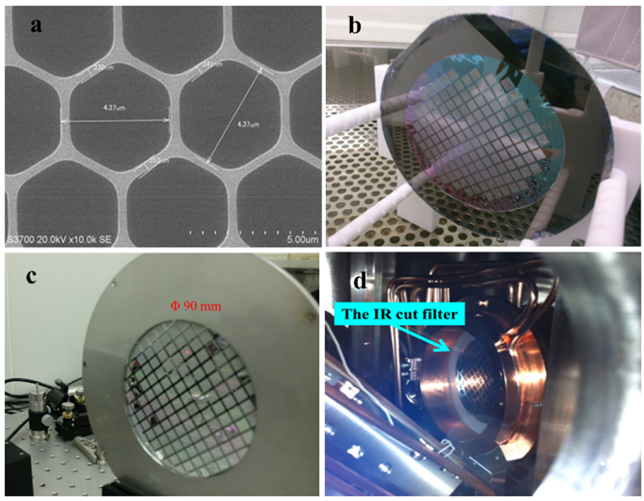


**Figure 6.** Grid transmissive SPF of IR suppression: (a) scanning electron microscopy image of the grid after etching, (b) grid SPF after backside wet etching, (c) grid SPF with a diameter of 90 mm installed for measurement and (d) grid SPF installed in the LPP source system. Adapted from Ref. [19].

mechanical strength is not ideal for high-power lasers, such as $Mo/MoSi_2$ multilayers[28].

To withstand a long-time heat load, a filter needs to have enough mechanical strength to ensure that it will not be broken by radiations. Bibishkina *et al.*[27] manufactured filters with different structures to improve the mechanical strength, such as a simple filter with a rigid framework, an improved structure with a mesh structure or a rigid mesh structure. However, these filters still cannot meet the requirements of commercial EUVL. To go further, Soer *et al.*[22] developed a honeycomb grid SPF with an EUV transmittance of 72% at normal incidence, which can stand a $CO_2$ laser power density of 100 W/cm$^2$ for 8 hours. Suzuki *et al.*[19] also adopted the honeycomb grid structure to produce an IR cut-off filter with a diameter of 90 mm for an EUV light source, as shown in Figure 6, and finally achieved 99.7% suppression for 10.6 μm, but the transmittance of EUV radiation is about 78%, which still leads to considerable EUV loss.

### *3.1.1. ASML's technical route*

In the EUVL system of ASML, the reticle is protected from being contaminated by covering a pellicle on it that has a higher reflectivity to DUV radiation than the BB, resulting in a greater impact on CD errors. To reduce its influence, a free-standing transmissive SPF, which is called a dynamic gas lock membrane (DGLm), is adopted by ASML in NXE:3400. Figure 7 depicts the details of the DGLm. The DGLm is mainly composed of four different layers[32], of which DUV and IR active layers are the core of the whole membrane to filter out the OoB radiations. Different from most transmissive SPFs' locations, the DGLm is located between the projection optics and the wafer. With this design, the DGLm acts as a physical barrier to prevent the contamination of projection optics caused by resistance outgassing[33]. The DGLm is a free-standing device, and thus it can be replaced once damaged. What is more, as the membrane is placed further away from the IF, it is less sensitive to non-uniform transmission and particles[32].

With the design of the DGLm, more than 99% DUV and nearly 80% IR radiations can be suppressed[32], as depicted in Figure 8. Since the total thickness of the membrane is below 50 nm and the absorption coefficient of the material is low, the EUV transmittance can reach 85%[32]. Without the DGLm, the CDs at the corners and edges are all less than 0.1 nm, which has already met the requirements of the N5 node, while with the DGLm, the CD reaches approximately 0.04 nm[16], which represents an improvement of DUV suppression. It should be noted that the excellent performance without the DGLm is based on the suitable solutions of other EUVL components, such as the specific designs of the BB and the sensitive enough resistance, but the DGLm can improve the DUV suppression under conditions that are not good enough, such as with less sensitive resistance. However, a potential problem is that the OoB light is not filtered until it enters the wafer stage; hence, the mirrors in the optical path will be damaged by the high-power radiation.

### *3.2. Reflective SPF*

The reflective SPF is designed to reflect EUV radiation, but diffract or absorb the OoB light. It is usually a composite grating structure with multilayers deposited on the surface. A typical study by Kierey *et al.*[34] manufactured a blazed grating SPF, which is composed of grating segments with different linear densities. The blazed grating is made of NG5 black glass and coated with an Ru layer. Its blazed angle is optimized to $1.2° \pm 0.2°$. One of the segments was measured on BESSY II, which showed that the EUV reflectivity reached 57% at the incident angle of 83°. The structure of the free-standing reflective SPF allows it to be designed onto the EUV collector, so the relevant researches on it are mainly focused on the early stage, which also provided a certain theoretical basis for the collector integrated with a grating structure. They will be discussed in combination with built-in SPFs in Section 4.

Comparing the above two SPFs, it can be found that the reflective SPF has better robustness and can be designed on the collector to reduce one optical element, although the EUV reflectivity may be limited to the collector efficiency (i.e., 70%). The advantage of the transmissive SPF is that it does not change the optical path of EUV radiation, so the design of the optic system has little or even no impact. Nevertheless, both two SPFs are free-standing devices that are easily broken by the OoB light, especially IR radiation. Therefore, built-in spectral purity filtering systems have been proposed and have become one of the mainstream schemes.

https://doi.org/10.1017/hpl.2023.53 Published online by Cambridge University Press

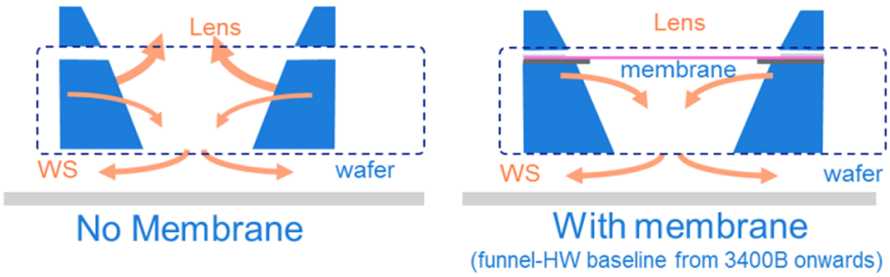


**Figure 7.** DGL's location and its influence on outgassing suppression. Reprinted from Ref. [31].

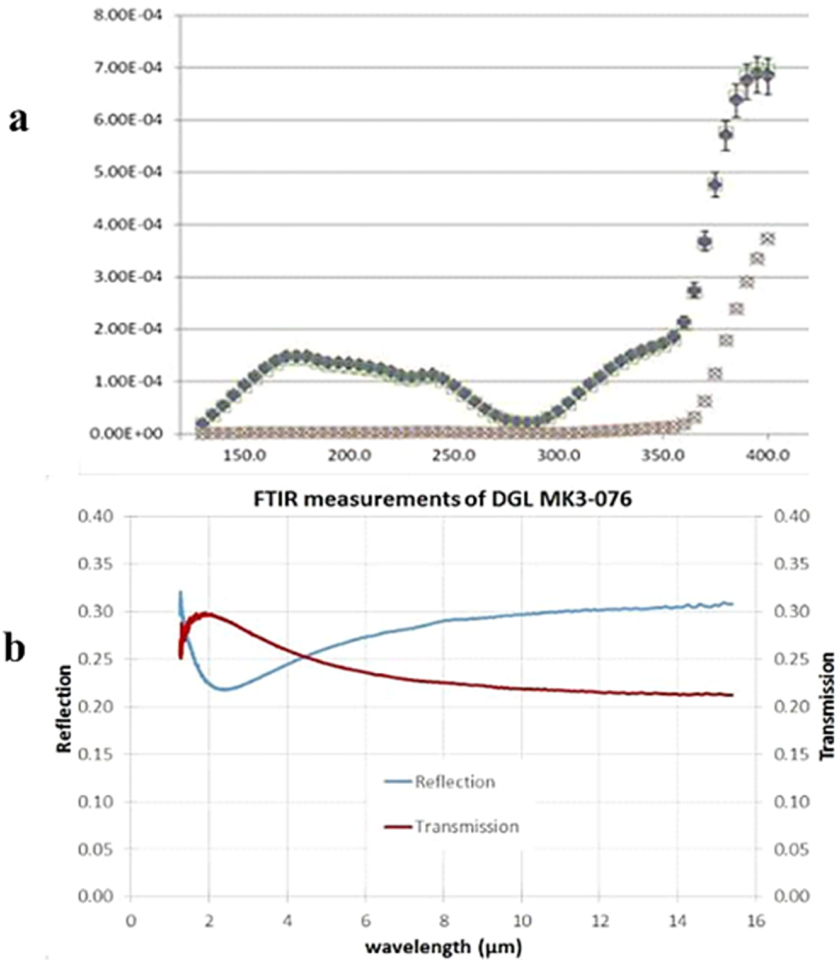


**Figure 8.** OoB suppression performance with DGLm: (a) complete suppression of DUV radiation (<0.1% transmitted) as measured by PTB; (b) 78% IR suppression as measured off-line by Fourier transform infrared spectroscopy. Adapted from Ref. [31].

## 4. Integrated spectral purity filters on the collector

The built-in SPF system refers to a collector integrated with grating structures, as shown in Figure 9. This design not only reduces an optical element in the light source system, but also has better mechanical strength, and the water-cooled device fabricated on the collector in some designs also reduces the thermal effect. There are mainly two technical routes of fabricating gratings on collectors[35]: one is to etch/deposit gratings on multilayers, which is introduced in Section 4.2, while the other is to fabricate gratings directly on the collector substrate, followed by coating, which is introduced in Section 4.3. The latter method is one of the mainstream methods, and has already been maturely applied to the EUVL light source system[8,36,37].

### *4.1. Principles*

The principles of the collector integrated with gratings are based on the Bragg reflection by the multilayers and the diffraction due to the predetermined grating shapes[38].

https://doi.org/10.1017/hpl.2023.53 Published online by Cambridge University Press

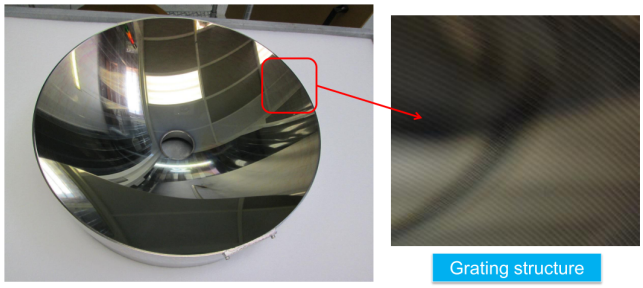


**Figure 9.** Collector with a grating structure from Gigaphoton, Inc. Reprinted from Ref. [15].

#### *4.1.1. Bragg diffraction*

The EUV collector is also known as a Bragg reflector[39] for the design of coating Mo/Si multilayers on the surface of the collector to maximize the EUV reflectivity. The Bragg reflector is an optical device that uses the constructive interference of reflected light at different interfaces to enhance the reflection of specific wavelengths[40,41]. According to the Bragg's law, when the optical path difference of the reflected light at two adjacent interfaces is half a wavelength, the reflected light at the interface will incur constructive interference and get a strong reflection[42]. The formula formation of Bragg's law in the case of periodic multilayers[43,44] is as follows:

$$2d\sin\theta = n\lambda, \tag{3}$$

where $d$ is the multilayer period, $\theta$ is the incident angle, $n$ is diffraction order and $\lambda$ is the incident wavelength. The reflectivity is determined by the number of layers and the refractive index difference between materials.

#### *4.1.2. Grating diffraction*

Grating diffraction is generally based on the Fraunhofer multi-slit diffraction effect. Once the optical path difference from the two adjacent slits to the interference point is an integral multiple of the wavelength of the incident light, the two beams have the same phase and the interference will be enhanced[40]. The grating equation summarizes the phenomenon:

$$p(\sin\delta + \sin\theta) = m\lambda, \tag{4}$$

where $p$ is the grating period, $\delta$ is the diffraction angle, $\theta$ is the incident angle, $m$ is the diffraction order and $\lambda$ is the wavelength of the incident light. With proper grating designs according to the grating equation, the needed radiation can be concentrated around one specific diffraction order, and most of the OoB radiation is diffracted to other orders[36,45,46].

Figure 10 shows the schematic of the OoB suppression design with the built-in SPF system, in which the blue line is the beam path of EUV radiation, while the red line is OoB radiation. After the laser radiations hit the Sn droplets, the EUV radiation is generated and the OoB radiations travel to the collector firstly. With the effect of the grating coated with Mo/Si multilayers, the EUV radiation concentrated at the zero order is reflected to the IF for the subsequent propagation, while the IR radiation is diffracted to higher diffraction orders and stopped by the beam stop.

### *4.2. Multilayer gratings*

The multilayer grating refers to etching/depositing multilayers in the shape of gratings on the substrate of the collector[48,49]. Spiller[50,51] first suggested using reflective multilayers to improve the EUV reflectivity of the grating[52]. Figure 11 depicts the schematic of the rectangular multilayer grating. The rectangular grating is not only easy to fabricate, but also effective to suppress the specific wavelength, and thus it is often considered as a good solution to the built-in SPF system. Van den Boogaard *et al.*[39] generated a

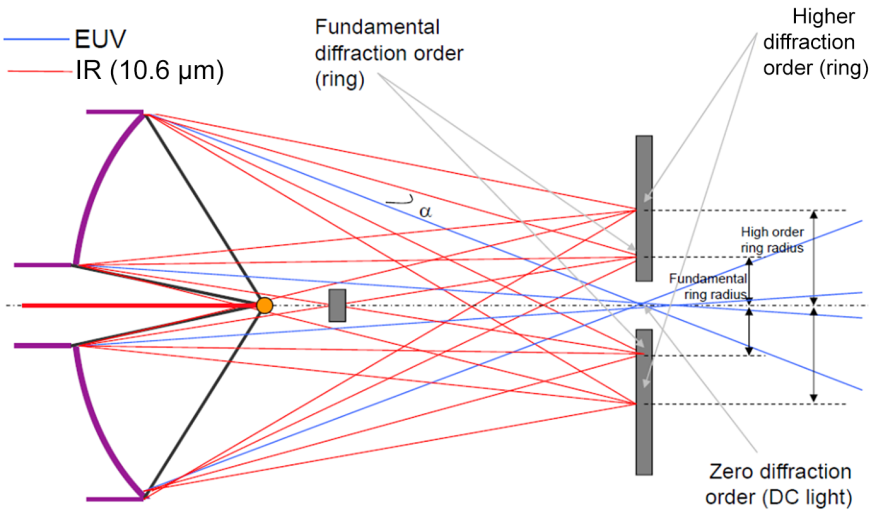


**Figure 10.** Schematic of the IR suppression design with the collector integrated with the rectangular substrate grating. Adapted from Ref. [47].

https://doi.org/10.1017/hpl.2023.53 Published online by Cambridge University Press

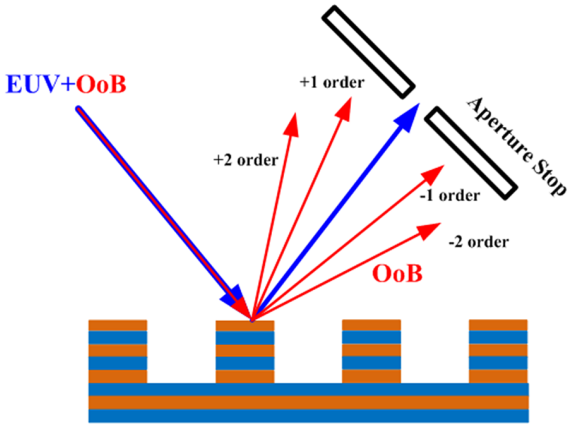


**Figure 11.** Schematic of the rectangular multilayer grating.

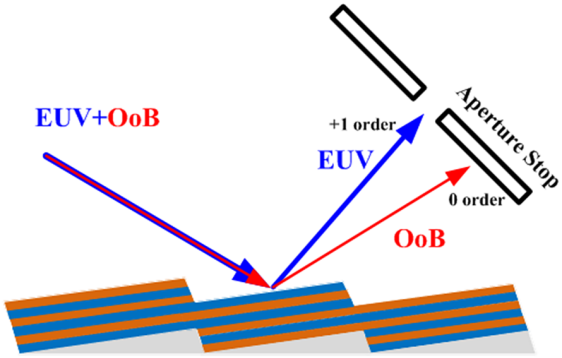


**Figure 12.** Schematic of the blazed multilayer grating.

Mo/Si rectangular multilayer grating reflector for EUVL that provided a 64% EUV reflectivity with a 30 times suppression at 280 nm. Trost *et al.*[49] designed a Mo/Si multilayer grating that generated only 0.04% IR radiation with an EUV reflectivity of 53% at zero order. Medvedev *et al.*[45] adopted the lift-off contact lithography process to fabricate the multilayer grating and achieved 61% EUV reflectivity with 70 times suppression at 10 μm. The process allowed a much shorter grating period to meet a better angular separation for EUV and OoB radiations. However, the rectangular multilayer grating can only be used to suppress a single wavelength, and is difficult to achieve high EUV diffraction efficiency (DE) while eliminating OoB radiation.

Compared with the rectangular grating, the blazed grating can suppress a wider range of wavebands[53], as shown in Figure 12. Naulleau *et al.*[54] analysed the main factors that affect the EUV and OoB efficiency in the EUVL light source system, and proposed a theoretical efficiency analysis of the blazed grating SPF. Van den Boogaard *et al.*[20] demonstrated theoretically that the full spectral separation can be obtained without losing EUV reflectance if the multilayer performance is not influenced by the process. Generally, the DE of the multilayer blazed grating is affected by the quality of the saw-tooth facets, smoothness of the substrate and groove density, and the former two are the main challenges. Naulleau *et al.*[52,55,56] proposed a method of fabricating the blazed grating and decreased the roughness caused by the substrate by smoothing the optimized multilayers, which presented an evident smoothing effect, while it was at the cost of the profile fidelity. Naulleau *et al.*[55] and Liddle *et al.*[57] identified the conditions for topography control while fabricating the blazed grating with hydrogen silsesquioxane (HSQ), and achieved a relative EUV efficiency of 63%. Voronov *et al.*[58] optimized the growth of Mo/Si multilayers by varying the sputtering gas pressure, and improved the DE from 39.6% to 44.0%. The same group[59] then founded that the reduction of the groove density and the high-order operation can lead to higher efficiency. A 52% EUV DE was obtained at the second order with a 2525 lines/mm blazed grating. Miles *et al.*[46] expounded the methodology of manufacturing the blazed grating and raised a way to replicate the grating, which obtained 65% DE at the first order. However, although numerous methods are raised to improve the process, it is still too difficult to meet the requirements, and thus the DE of the blazed grating is far from the theoretical limit.

A new pyramid structure with a feasible process method, such as half-shadowing, has been proposed to suppress the full DUV band, as shown in Figure 13. Initially, a 2D pyramid structure made of Si that was deposited on Mo/Si multilayers was preferred. Huang *et al.*[61] studied the mechanism of a pyramid structure suppressing DUV radiation, and the Si pyramid showed 0.1%–10.5% DUV reflectivity, which was about 14 times suppression compared with the non-structured collector, and the EUV's peak reflectivity reached 56.2%. To reduce the loss of EUV radiation, the Mo/Si multilayer pyramid was proposed to replace the Si pyramid and the EUV reflectivity was up to 64.7%, while the DUV response was the same as that of the Si pyramid[48,60]. Although the multilayer pyramid grating shows good performance within DUV filtering and EUV reflectivity, this structure has not been made and tested on the EUVL collector to the authors' knowledge, and the performance in IR filtering also has not been studied.

The multilayer grating provides a method to integrate the grating structure with the collector, and has been widely studied in recent years. The key point, as well as the difficulty, of this technology is to develop a suitable process for stacking multilayers without degrading the EUV reflectivity[62]. In particular, the rectangular grating on the collector requires about 500 pairs of layers[49,62] with smooth surfaces, steep edges, etc., and this largely reduces the feasibility of using multilayer gratings as the SPF.

### *4.3. Substrate gratings*

The substrate grating refers to the case in which the surface of the collector substrate is firstly fabricated in the shape of the grating, and then the multilayers are deposited[35,62].

https://doi.org/10.1017/hpl.2023.53 Published online by Cambridge University Press

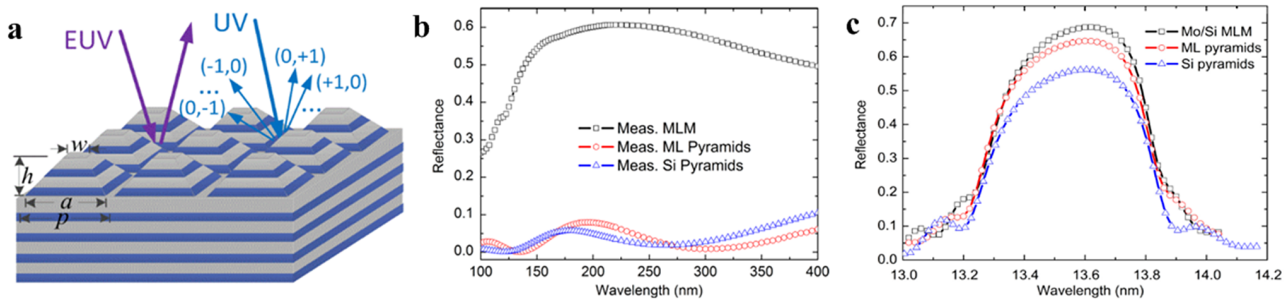


**Figure 13.** 2D pyramid multilayer grating on the collector: (a) design of the multilayer pyramids; (b) UV-suppression performance of Si pyramids and the Mo/Si multilayer mirror in (a); (c) EUV performance comparison of Si pyramids and the Mo/Si multilayer mirror in (a). Adapted from Refs. [53,60].

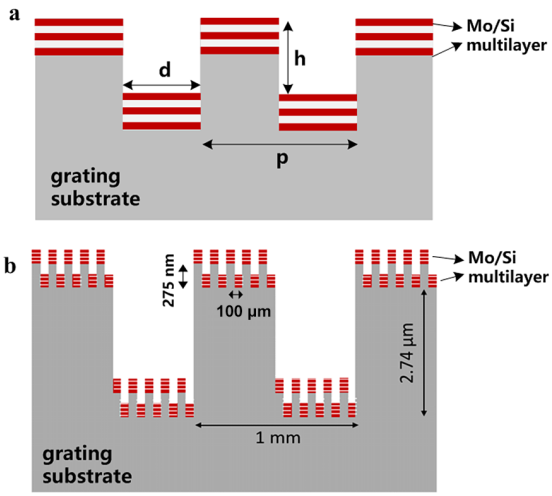


**Figure 14.** Design of the rectangular substrate grating: (a) schematic of 1D rectangular substrate grating; (b) schematic of 2D rectangular substrate grating by IOF. Adapted from Refs. [53,62].

The method has advantages. It reduces an optical element in the light source system, has a good mechanical strength and avoids the process difficulty of stacking hundreds of layers. This scheme has already been applied to the collector by Gigaphoton, Inc.[37,63–65]. They adopted the rectangular grating as the substrate grating to filter out the IR radiation of 10.6 μm and 1064 nm, and achieved only 0.37% IR reflectivity[47,66], while the EUV reflectivity only reduced by approximately 4% compared with the mirror without a grating structure[37].

This section will mainly discuss the rectangular substrate grating, including the design principles, fabrication process and the metrology. Gratings of other shapes will also be introduced briefly as a supplement in Section 4.3.4.

### *4.3.1. Design principles*

Assume that the OoB radiation that needs to be suppressed is 10.6 μm and the grating is in the shape of a 1D rectangle. As Figure 14 shows, the grating is characterized by the period $p$, width $d$ and depth $h$ of the grooves. When the 13.5 nm EUV radiation combined with the 10.6 μm is incident onto the grating, if the diffraction order $m = 0$, both radiations' reflection angles are the same, while with higher diffraction orders, the characteristic values of the diffraction angles differ by about three orders of magnitude[45]. Therefore, the 10.6 μm radiation at $m = 0$ is what we need to suppress. Assuming that the grating is illuminated by the normal-incidence plane wave, the following equation shows the $m$th-order DE of the 1D rectangular phase grating:

$$R_n = R_{\text{tot}}|\text{sinc}\,(m\pi) + A\Gamma\,\text{sinc}\,(m\pi)|^2, \tag{5}$$

where $R_{\text{tot}}$ is the total reflected intensity, $\Gamma = \frac{d}{p}$ and $A = \exp\left(\frac{i\cdot 4\pi h}{\lambda}\right) - 1$, and

$$R_0 = R_{\text{tot}}\left\{1 + 2\Gamma\,(\Gamma - 1)\left[1 - \cos\left(\frac{4\pi h}{\lambda}\right)\right]\right\} \tag{6}$$

is the particular case of zero diffraction order, which both can be derived from Equation (2)[45]. To suppress the 10.6 μm IR radiation at zero order, Equation (5) should be equal to zero. It can be calculated that the fill factor $\Gamma = 0.5$ and the minimum depth of the grooves is $h = \frac{\lambda}{4} = \sim 2.65$ μm. The period $p$ is more difficult to determine because it is a trade-off between IR reflectivity at the zero order ($\sim p/\lambda$) and the angular separation of diffraction ($\sim \arcsin(\lambda/p)$)[45,67]. What is more, the limited spatial and temporal coherence of the radiation should also be considered[45,60].

To suppress radiations of two wavelengths, in particular 10.6 μm and 1064 nm, this method can be used to determine the dual-layer grating. Since the difference between the two wavelengths is 10 times, the parameters of the grating are also 10 times different. The Fraunhofer Institute for Applied Optics and Precision Engineering (IOF)[36,62] designed and fabricated a dual-wavelength rectangular grating with optimized geometric parameters, as shown in Figure 14. At the IF, the measured reflectivity of 10.6 μm is 0.32%, the reflectivity of 1064 nm is only 0.08% and the average reflectivity of the EUV radiation at 13.5 nm is 64% which represents only 4.5% loss compared to the unstructured multilayers.

https://doi.org/10.1017/hpl.2023.53 Published online by Cambridge University Press

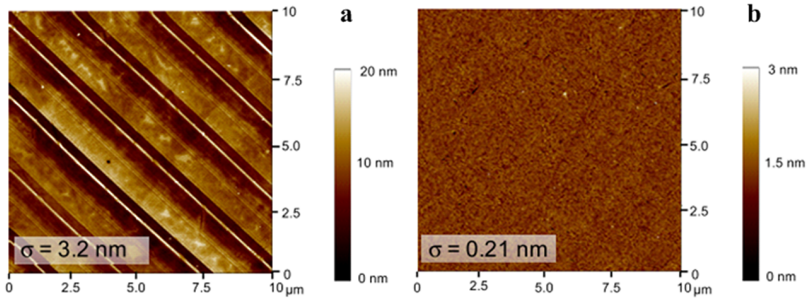


**Figure 15.** (a) AFM image of diamond-turned patterns and (b) the mechanical polished surface of (a). Reprinted from Ref. [49].

*4.3.2. Fabrication process*

At present, there are two main processes to fabricate the substrate gratings deposited with multilayers. The main difference between them is the preparation of the substrate grating, which involves the diamond turning process and ion beam etching.

The process of manufacturing the substrate grating used by Rigaku is the diamond turning[15]. Firstly, Ni is injected into the substrate made of Al alloy and the surface of it is polished. Then the grating grooves are made on the Ni surface by diamond turning, which will result in turning patterns, as shown in Figure 15(a), and high spatial frequency roughness (HSFR) on the cut surface. Therefore, a glass smoothing layer is then needed to smooth the substrate grating. The other method, the ion beam etching process, is used by IOF[36,62] to prepare a dual-layer rectangular grating on the collector's substrate, which is made of AlSi alloy. With the method, the substrate is firstly diamond turned and polished to reduce the HSFR to less than 0.2 nm rms, and then, the dual-layer grating is directly constructed into the NiP layer of the AlSi substrate by ion beam etching.

When manufacturing the substrate grating, the HSFR is a critical factor to achieve a smooth enough surface. To reduce the HSFR, some methods are proposed. Mechanical polishing[49] is the simplest smoothing method, which is mainly used to remove typical diamond turning structures. As shown in the Figure 15, it reduced the HSFR by more than 10 times. Ion beam polishing technology[68,69], which is commonly used on collectors without gratings, uses the neutral ion beam to bombard the workpiece, removing atoms or molecules in a certain area of the surface, and achieves ultra-smooth polishing. The method of adding a smoothing layer[70] refers to manufacturing a film on the substrate with a smaller HSFR to smooth the roughness, and the performance can be seen in Figures 16(a) and 16(b). Stock *et al.*[71] used the electron beam evaporation method to deposit a

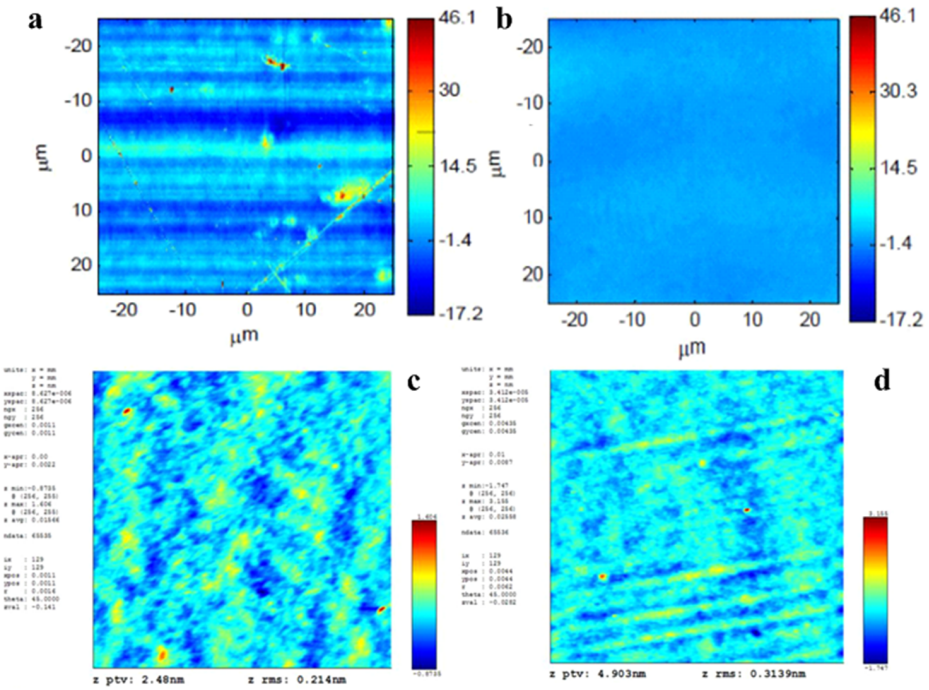


**Figure 16.** HSFR results (AFM) of adding a smoothing layer by Rigaku: (a) diamond-turned surface sample; (b) smoothed diamond-turned surface sample; (c) 0.14–0.29 nm rms over 2.2 μm scans; (d) 0.29–0.39 nm rms over 8.7 μm scans of the grating surface. Adapted from Refs. [8,15].

https://doi.org/10.1017/hpl.2023.53 Published online by Cambridge University Press

single layer of carbon on the substrate of BK7 and Zerodur to smooth the roughness. Salmassi *et al.*[72,73] proposed a spin-on-glass resistance process based on HSQ to smooth a substrate with diamond-turned structures and presented a roughness reduction from 3.7 nm to 0.39 nm rms on the Al substrate. Rigaku[8] used a glassy smoothing layer on the substrate grating to reduce the HSFR of the surface, achieving the results presented in Figures 16(c) and 16(d), which is sufficient for high performance. Ulmer *et al.*[74] designed a mirror with a diameter of 1 m and smoothed the NiP substrate by covering the $CN_x$ layer.

### *4.3.3. Metrology*

During the preparation of the substrate grating, some measurements are needed to measure the machining accuracy and the overall device performance. The three main aspects to be measured are the roughness, reflectivity for different wavelengths and uniformity of reflectivity.

**Roughness.** The thickness of the multilayers deposited on the substrate grating is at the level of nanometres, and thus the morphology and roughness of the substrate will be translated to the top layers[55,70,75]. It is clear that the prerequisite for reducing the roughness of the multilayers is to reduce the roughness of the substrate grating. The evaluation indicators for roughness include the average roughness, root mean square (RMS) roughness, peak-to-valley (PV) value, power spectral density (PSD), etc. The first three are simple statistical parameters and only the vertical component of surface roughness is calculated[70]. The PSD measures the roughness from the perspective of Fourier spectra, thereby obtaining the spatial frequency distribution of the surface error, which means it also contains the transverse and longitudinal information of the surface[76,77].

Roughness in different spatial frequency ranges should be measured by different methods, as shown in Figure 17. According to the scattering theory, the scattering caused by roughness in different spatial frequencies can be generally divided into the following three types[75,78–80]:

(1) minimum angle scattering caused by low spatial frequency roughness (LSFR), which introduces basic aberration into the system, will blur the image and reduce the resolution of the optical system;

(2) small-angle scattering caused by medium spatial frequency roughness (MSFR), also known as stray light, will reduce the contrast of spatial imaging;

(3) large-angle scattering caused by HSFR will reduce the light flux reaching the image plane, thus reducing the energy transmission efficiency of the optical system.

Taking Rigaku's work as a reference[8], the different spatial frequencies of roughness, corresponding to the above influences, are defined as follows: LSFR, more than or equal to 1 mm; MSFR, 1 mm–10 μm; HSFR, less than or equal to 10 μm.

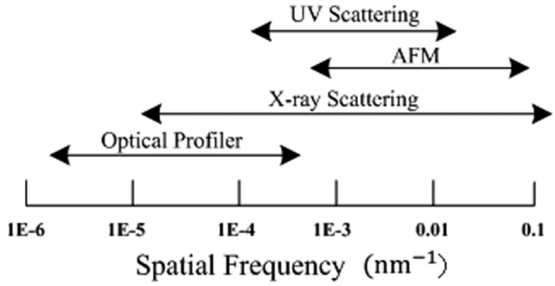


**Figure 17.** Different measurements for roughness at different spatial frequencies. Adapted from Ref. [70].

The HSFR is a critical indicator to be measured because among the roughness in all frequency bands, the roughness with the spatial wavelength equivalent to the incident light wavelength has the strongest scattering ability[70]. The HSFR of the grating surface used for the collector needs to be less than 0.3 nm rms[49,62], which is also the main challenge of the fabrication. At present, the main and most direct method used in HSFR for measuring surfaces with less than or equal to 0.1 nm rms is atomic force microscope (AFM) measurement, which determines the distance between the probe and the detection surface by the contact force. Its detection area is usually less than tens of micrometres, the longitudinal resolution is approximately 0.01 nm[77] and the transverse resolution can generally be up to 0.1 nm[70,76], which depends on the radius of curvature of the probe and the depth from the top of the probe to the detection surface[70,81]. In the IOF's experiments on the dual-layer rectangular grating[36,82], with a scanning range of 10 μm × 10 μm, the roughnesses of the four facets of the grating were all below 0.25 nm rms. It should be noted that if PSD is used for characterization, it is necessary to measure the same surface at different locations and meet the sampling theorem.

The LSFR is primarily measured by optical profilometry, including white light interferometry (WLI), double-beam interferometry, etc., among which WLI is the main method currently used. WLI is a non-contact metrology, and has the advantages of a large measuring range, high vertical accuracy and fast measuring speed. Based on the principle of optical interference, WLI can analyse the relative height variation of the sample surface according to the contrast and position of the light interference fringe, thus generating a 3D image and obtaining the 3D morphology and surface roughness of the measured sample. However, due to the influence of dispersion, its lateral accuracy can only reach the scale of hundreds of nanometres[76,77]. The IOF[36] used the WLI to characterize the profile of its dual-layer substrate grating, as Figure 18 shows, and controlled the maximum error of the grating period, fill factor and groove depth within less than 1%. Rigaku[8] also used an interference microscope to

https://doi.org/10.1017/hpl.2023.53 Published online by Cambridge University Press

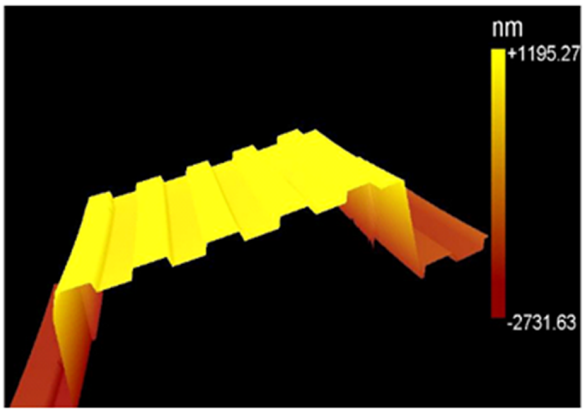


**Figure 18.** WLI analysis of a dual-layer rectangular substrate grating structure by the IOF. Reprinted from Ref. [62].

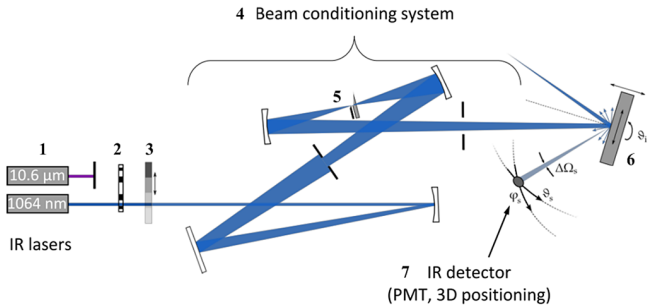


**Figure 19.** ARS instrument ALBATROSS for scattering measurements in the UV-VIS-IR range. Components include laser sources (1), mechanical chopper for lock-in amplification (2), attenuation filters (3), beam preparation optics (4), polarizer (5), sample (6) and detector (7). Adapted from Ref. [62].

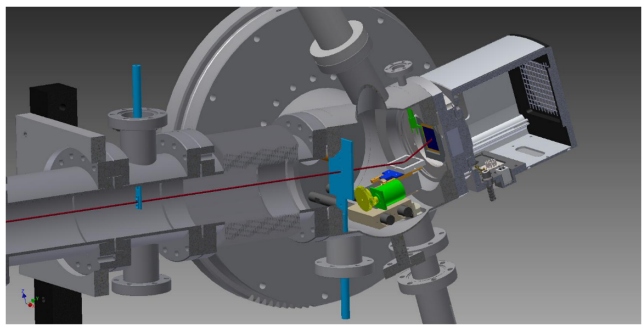

**Figure 20.** EUV-ARS for the characterization of nanometre structures exposed by PTB. Reprinted from Ref. [87].

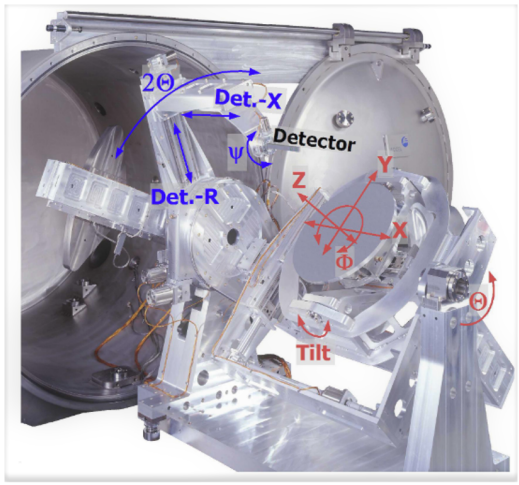


**Figure 21.** Mechanics of the EUV reflectometer by PTB. Reprinted from Ref. [89].

measure the roughness of the substrate grating, and achieved an LSFR of 0.577 μm rms.

The MSFR can be measured by laser speckle interferometry and light scattering measurement, both of which are indirect measurement. The former is primarily used in the detection range where the roughness is greater than the illumination wavelength[70], and has the advantages of simple operation and a large measurement range. The brightness, shape and contrast of the speckles generated by the coherent wave can effectively reflect the distribution of surface roughness. Light scattering measurement mainly includes the angle resolved scattering (ARS) measurement and total integrated scattering (TIS) measurement[83]. ARS determines the roughness according to the distribution of the scattered light intensity in the plane[84], while TIS determines the roughness according to the ratio of the light intensity in the hemisphere to the light intensity reflected on the surface of the sample[85]. Compared with TIS, ARS is more complex and expensive, but it can correctly measure the spatial distribution of scattered light and obtain more roughness information[83]. Trost *et al.*[49] used ALBATROSS (Figure 19), developed by the IOF, to measure the roughness of the multilayer grating. Hilpert *et al.*[86] measured the roughness of the reflector in the spaceborne optical system by ARS and obtained a roughness value of 0.1 nm rms. Herrero *et al.*[87] of Physikalisch-Technische Bundesanstalt (PTB) exposed a new tool (EUV-ARS) based on the grazing incidence small-angle X-ray scattering instrument (Figure 20), which allows one to study the structural surface by analysing the scattered light and fluorescence signals, and to achieve the roughness measurement at the nanoscale.

**OoB suppression and EUV reflectivity.** The collector integrated with rectangular gratings is designed to suppress 10.6 μm and 1064 nm IR radiation without reducing EUV radiation, so it is necessary to detect the intensity of EUV and IR radiations at the focal plane. Compared with the collector without the grating structure, the intensity of IR radiation at the IF generally needs to be suppressed by more than 99%[12], while the minimum loss of EUV radiation achieved nowadays is approximately 4.81%[88].

For the EUV detection, the equipment used includes the EUV reflectometry at BESSY II developed by PTB in Germany[89–92] (Figure 21), the EUV reflectometry by the National Institute of Standards and Technology (NIST) in the USA[93] and the system MERLIN of the IOF[94].

https://doi.org/10.1017/hpl.2023.53 Published online by Cambridge University Press

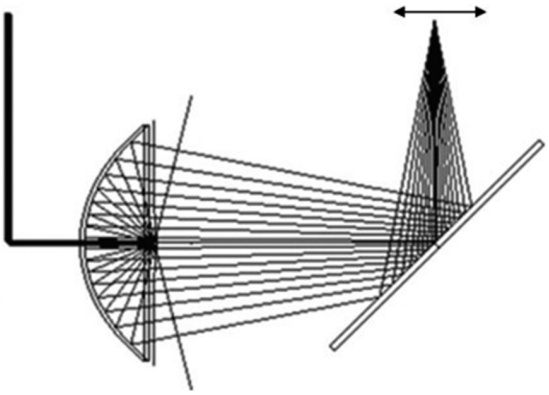

**Figure 22.** Schematic of the IR suppression test stand. Reprinted from Ref. [8].

For the detection of IR suppression, ALBATROSS[95] can also be used. In fact, ALBATROSS is a device that can measure the reflected light, transmitted light and scattered light distribution with a high dynamic range, high sensitivity and low noise. What is more, the measurement device can also be custom-built for the actual measuring needs, as shown in Figure 22. The laser firstly passes through the beam expander, chopper, etc., and is then reflected by the virtual light source sphere before being incident on the full-size collector. After being deflected by a folded plane mirror, it is focused on the HgCdTe detector for the measurement[8].

**Reflectivity uniformity.** The final step in the preparation of the substrate grating is to deposit Mo/Si multilayers, which aims to improve the EUV reflection performance, so measuring the EUV reflectivity uniformity is very important. The EUV reflectometry mentioned above is used to symmetrically select multiple positions on the collector's surface along the *x*- and *y*-axes and measure their reflectivity for comparison. The IOF[36] used the system of PTB to compare the average EUV reflectivity of the collector integrated with the dual-layer grating, and the change of EUV reflectivity is approximately 0.5%. Rigaku[8] used the same system as the IOF to measure the peak EUV reflectivity of the collector surface, and showed a variation of less than 0.0025 nm at the opposite positions, referring to 0.02% PV variation.

### *4.3.4. Gratings with other shapes*

According to the existing technical schemes, the collector substrate of the rectangular grating structure cannot effectively filter the DUV radiation, so it is proposed to use a blazed grating to replace the rectangular grating since the structure was theoretically demonstrated to be effective at filtering out full-OoB radiations by van den Boogaard *et al.*[20] when studying the multilayer grating.

Johnson[67,96] designed a collector integrated with the blazed grating structure that aims to divert the EUV radiation into the IF rather than diffracting IR radiation out of the

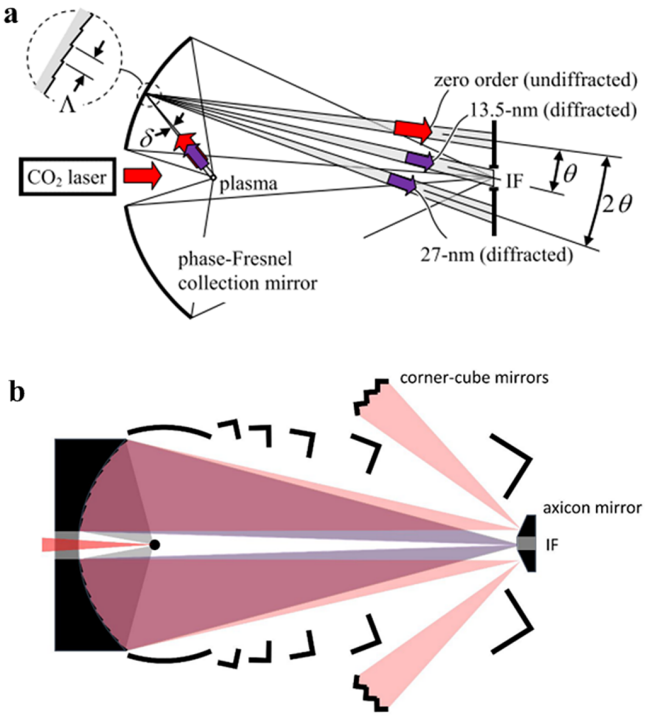


**Figure 23.** (a) Schematic of the collector integrated with the blazed substrate grating and (b) schematic of the collector with power recycling mirrors. Reprinted from Refs. [96,97].

IF, as shown in Figure 23(a), and two fabrication methods are given, which are the conformal-multilayer grating and patterned-multilayer grating. What is more, a power recycling component was designed surrounding the IF aperture to retroreflect IR radiation for a higher source conversion efficiency (CE). Following that, Hassanein *et al.*[97] continued the design of the blazed grating and furthered the idea of power recycling, which showed a potential 60% gain of EUV-CE with the preliminary plasma simulation, as shown in Figure 23(b). However, these relevant researches based on the substrate blazed grating are mainly theoretical analyses, and no experiments have been carried out to establish the feasibility of this scheme.

Theoretically, the blazed grating can indeed suppress the radiation of the IR and UV bands, but the problem lies in the limitations of the manufacturing process. For example, it is difficult to control the blazed angle of the multilayers within 3°[35]. Therefore, its actual effect is far from reaching the theoretical effect, so it is still at the theoretical stage.

## 5. Conclusions and expectations

As the most precise manufacturing process in the world today, lithography technology imposes very high requirements for the purity of its high-power EUV light source. For the LPP-EUVL system, the OoB radiation with the greatest impact is IR radiation (i.e., 1064 nm and 10.6 μm) and DUV

https://doi.org/10.1017/hpl.2023.53 Published online by Cambridge University Press

radiation, the former of which causes the thermal effect and reduces the pattern accuracy, while the latter leads to CD errors. Therefore, the intensity of IR radiation needs to be less than 10% and that of DUV radiation needs to be only 1% of that of EUV radiation at the wafer to avoid potential damage, while the intensity of EUV radiation must be as high as possible.

Taking the above conditions as the basic indicators for evaluating the SPF for EUVL, it can be found that traditional free-standing SPFs can barely satisfy the suppression requirements of IR and DUV radiations, and also lead to an EUV loss of approximately 30%[88]. However, some new free-standing filters have been proposed in recent years and have shown a good performance, such as the DGLm by ASML, which suppressed 99% of DUV radiation and 80% of IR radiation, while the EUV transmittance reached 85%. Although it may have problems of non-ideal mechanical strength and an extra optical element, it still shows potential as an SPF for EUVL, especially for the suppression of DUV radiation, as it produces less thermal damage to the optical elements, compared to IR radiation.

The scheme of taking the micro-structures, integrated onto the collector, as the SPF for an EUVL light source also seems to be feasible and effective, especially the substrate grating structure, which avoids the process difficulty of stacking thousands of layers. According to the achievements of current researches, Gigaphoton, Inc., has already obtained an IR suppression of 0.37% at the IF, while the reduction of EUV reflectivity with an unpolarized incident laser is only around 4% compared with the non-structured collector, which represents a better performance than free-standing SPFs. Besides that, this scheme allows a superior mechanical strength, and some designs can be applied onto the collector to relieve the thermal effect, such as a water-cooled device.

The existing designs of the collector integrated with the substrate grating still need to be optimized. For the rectangular grating, which has been studied maturely, it only suppresses finite and specific wavelengths, and there is no research showing its suppression capacity in the DUV band so far. Therefore, how to suppress IR radiation at the same time as DUV radiation is a problem that remains. There are probably three ways to go. One is to adopt the scheme of integrating the collector with the blazed substrate grating. This method raises difficulties of stacking lots of layers, which has been the challenge for years and, also, manufacturing the periodic blazed grating on such a large collector is not easy. The second is to further develop the membrane that is manageable to suppress all OoB radiations, just like DGLm, but this faces the problem of being broken easily by the thermal effect from the $CO_2$ laser and will increase the cost of maintenance. The third is to combine the other two schemes, which means integrating the collector with rectangular gratings, while using a transmissive SPF membrane. A similar method has been explored by Suzuki *et al.*[19], but they use two free-standing SPFs (one for IR radiation and one for DUV radiation), which obviously represents less mechanical strength than the collector. Thus, there is still room for the improvement of the spectral purity of the EUV light source.

Besides the designs of SPFs for the EUVL light source, the metrology also needs to be improved. With the development of the semi-industry, metrologies that can deal with the smaller and more complex nano-structures are needed. There is no doubt that the scattering metrology plays an important role in this field. To achieve a higher sensitivity, grazing incidence small-angle X-ray scattering is often used, but it has the problem of large footprints of the beam, which needs to be resolved in a more general solution. Using a larger incident wavelength as the source, which allows a larger incident angle, may relieve this problem without reducing the sensitivity. Herreroa *et al.*'s work[87] gives some suggestions in this aspect. Another problem that limits the performance of the measuring is the speed of the measurement; in particular, when measuring the surface roughness, the ARS needs a lot of time to detect the scattering distribution in the hemisphere space, which can be relieved by the improvement of the scattering model to some extent, such as the regional scattering model by Wang *et al.*[98]. Efforts shall be made on the design of the measuring devices as well as the metrologies in order to meet the requirements of measuring nano-structures.

This paper reviews the development of the SPFs for EUVL, and investigates the key technologies of filtering out OoB radiations for EUVL. The main challenges and developing trends are also discussed in view of the practical applications for further improvement. It can be seen that the design and manufacture of SPFs for EUVL is not a single task; rather, it requires a coordinated advancement in design methods, process manufacturing and metrologies.

## Acknowledgement

This work was supported by the Science and Technology Commission of Shanghai Municipality (No. 22DZ1100300).

## References

1. G. E. Moore, https://www.computerhistory.org/collections/catalog/102 (1965).
2. J. W. S. Rayleigh, *The Theory of Sound* (Dover Publications, New York, 1945).
3. N. Zong, W. M. Hu, Z. M. Wang, X. J. Wang, S. J. Zhang, Y. Bo, Q. J. Peng, and Z. Y. Xu, Chin. Opt. **13**, 28 (2020).
4. T. Tomie, J. Micro-Nanolith. MEM **11**, 021109 (2012).
5. Y. Teramoto, B. Santos, G. Mertens, R. Kops, M. Kops, A. van Wezyk, H. Yabuta, A. Nagano, T. Shirai, N. Ashizawa, K. Nakamura, and K. Kasama, Proc. SPIE **9422**, 94220F (2015).
6. N. Lin, W. H. Yang, Y. Y. Chen, X. Wei, C. Wang, J. L. Zhao, Y. J. Peng, and Y. X. Leng, Laser Optoelectron. **59**, 0922002 (2022).
7. I. Fomenkov, A. Schafgans, and D. Brandt, Synchrotron Radiat. News **32**, 3 (2019).

https://doi.org/10.1017/hpl.2023.53 Published online by Cambridge University Press

8. M. Kriese, Y. Platonova, B. Ehlersa, L. Jianga, J. Rodrigueza, U. Muellerb, J. Danielb, S. Khatrib, A. Magruderb, S. Granthamc, C. Tarrioc, and T. Lucatortoc, Proc. SPIE **9048**, 90483C (2014).
9. B. Rollinger, "Droplet target for laser-produced plasma light sources," PhD. Thesis (ETH Zurich, 2010).
10. V. Bakshi, *EUV Lithography* (SPIE Press, Bellingham, WA, 2018).
11. D. K. Yang, D. Wang, Q. Huang, Y. Song, J. Wu, W. Li, Z.-S. Wang, X. Tang, H. Xu, S. Liu, and C. Gui, Chip **1**, 100019 (2022).
12. V. Bakshi, *EUV Sources for Lithography* (SPIE Press, Bellingham, WA, 2006).
13. C. Wagner and N. Harned, Nat. Photonics **4**, 24 (2010).
14. F. Liu, F. van de W. M. Bayraktar, F. Bijkerk, D. Smeets, S. Huang, Y. Ni, A. Yakunin, P. Havermans, R. Oesterholt, F. Torretti, J. Scheers, and O. Versolato, in *2019 EUVL Workshop* (2019).
15. Y. Platonov, M , Kriese, R. Crucet, Y. Li, V. Martynov, L. Jiang, J. Rodriguez, U. Mueller, J. Daniel, S. Khatri, A. Magruder, S. Grantham, C. Tarrio, and T. B. Lucatorto, in *2013 EUVL Sources Workshop* (2013).
16. M. van de Kerkhof, F. Liu, M. Meeuwissen, X. Zhang, R. de Kruif, N. Davydova, G. Schiffelers, F. Waelisch, E. van Setten, W. Varenkamp, K. Ricken, L. de Winter, J. McNamara, M. Bayraktar, N. M. Felix, and A. Lio, Proc. SPIE **11323**, 1132321 (2020).
17. M. van de Kerkhof, F. Liu, M. Meeuwissen, X. Zhang, M. Bayraktar, R. de Kruif, and N. Davydova, J. Micro-Nanolith. MEM **19**, 033801 (2020).
18. M. Bayraktar, F. A. van Goor, K. J. Boller, and F. Bijkerk, Opt. Express **22**, 8633 (2014).
19. Y. Suzuki, K. Totsu, M. Moriyama, M. Esashi, and S. Tanaka, Sens. Actual A: Phys. **231**, 59 (2015).
20. A. J. R. van den Boogaard, E. Louis, F. A. van Goor, and F. Bijkerk, Proc. SPIE **7271**, 72713B (2009).
21. C. M. Park, I. Kim, S. H. Kim, D. W. Kim, M. S. Hwang, S. N. Kang, C. H. Park, H. W. Kim, J. H. Yeo, and S. S. Kim, Proc. SPIE **9048**, 90480S (2014).
22. W. A. Soer, M. J. J. Jak, A. M. Yakunin, M. M. J. W. Herpen, and V. Y. Banine, Proc. SPIE **7271**, 72712Y (2009).
23. S. A. George, P. P. Naulleau, S. Rekawa, E. Gullikson, and C. D. Kemp, Proc. SPIE **7271**, 72710X (2009).
24. G. F. Lorusso, N. Davydova, M. Eurlings, C. Kaya, Y. Peng, K. Feenstra, T. H. Fedynyshyn, O. Natt, P. Huber, C. Zaczek, S. Young, P. Graeupner, and E. Hendrickx, Proc. SPIE **7969**, 79692O (2011).
25. O. Romanets, K. Ricken, M. Kupers, F. Wahlisch, C. Piliego, P. Proman, D. de Graaf, U. F. Behringer, and J. Finders, Proc. SPIE **11177**, 111770Z (2019).
26. G. Salmaso and R. Maas, Proc. SPIE **11854**, 118540R (2021).
27. M. S. Bibishkin, N. I. Chkhalo, S. A. Gusev, E. B. Kluenkov, A. Y. Lopatin, V. I. Luchin, A. E. Pestov, N. N. Salashchenko, L. A. Shmaenok, N. N. Tsybin, and S. Y. Zuev, Proc. SPIE **7025**, 702502 (2007).
28. N. I. Chkhalo, A. A. Orlikovsky, M. N. Drozdov, E. B. Kluenkov, A. Y. Lopatin, V. I. Luchin, A. E. Pestov, N. N. Salashchenko, L. A. Shmaenok, and N. N. Tsybin, Proc. SPIE **7521**, 752105 (2009).
29. S. S. Andreev, E. B. Kluenkov, A. Y. Lopatin, V. I. Luchin, K. A. Prokhorov, N. N. Salashchenko, L. A. Suslov, and S. Y. Zuev, Poverhnost **N2**, 6 (2003).
30. N. I. Chkhalo, M. N. Drozdov, E. B. Kluenkov, A. Y. Lopatin, V. I. Luchin, N. N. Salashchenko, N. N. Tsybin, L. A. Sjmaenok, V. E. Banine, and A. M. Yakunin, J. Micro-Nanolith. MEM **11**, 021115 (2012).
31. I. Fomenkov, in *International Workshop on EUV Lithography* (2017).
32. M. van de Kerkhof, H. Jasper, L. Levasier, R. Peeters, R. van Es, J.-W. Bosker, A. Zdravkov, E. Lenderink, F. Evangelista, P. Broman, B. Bilski, and T. Last, Proc. SPIE **10143**, 101430D (2017).
33. R. Es, M. van de Kerkhof, A. Minnaert, G. Fisser, J. Klerk, J. Smits, R. Moors, E. Verhoeven, L. Levasier, R. Peeters, M. Pieters, and H. Meiling, Proc. SPIE **10583**, 105830H (2018).
34. H. Kierey, K. Heidemann, B. Kleemann, R. Winters, W. E. W. Singer, F. Melzer, R. Wevers, and M. Antoni, in *Advances in Mirror Technology for X-Ray, EUV Lithography, Laser, and Other Applications* (Academic, Bellingham, WA, USA, 2004), p. 70.
35. L. C. Zhang, OME Inform. **28**, 5 (2011).
36. T. Feigl, M. Perske, H. Pauer, T. Fiedler, U. Zeitner, R. Leitel, H.-C. Eckstein, P. Schleicher, S. Schröder, M. Trost, S. Risse, R. Steinkopf, F. Scholze, and C. Laubis, Proc. SPIE **9422**, 94220E (2015).
37. H. Nakarai, T. Abe, H. Tanaka, Y. Watanabe, T. Hori, T. Kodama, Y. Shiraishi, T. Yanagida, G. Soumagne, T. Yamada, and T. Saitou, in *4th Fraunhofer Symposium on Digital Photonics Made in Germany* (2019).
38. M. Moriya, O. Wakabayashi, and G. Soumagne, U.S. patent 8,592,787,B2 (November 26, 2013).
39. A. J. R. van den Boogaard, F. A. van Goor, E. Louis, and F. Bijkerk, Opt. Lett. **37**, 160 (2012).
40. C. Kittel and P. McEuen, *Introduction to Solid State Physics* (John Wiley & Sons, Singapore, 2018).
41. A. Haase, *Multimethod Metrology of Multilayer Mirrors Using EUV and X-Ray Radiation* (Technische Universitaet, Berlin, 2017).
42. S. Migura, https://www.euvlitho.com/2019/P24.pdf (2019).
43. K. L. Guen, J. M. André, M. Wu, V. Ilakovac, F. Delmotte, S. de Rossi, F. Bridou, E. Meltchakov, A. Giglia, and S. Nannarone, J. Nanosci. Nanotechno. **19**, 593 (2019).
44. H. G. J. Moseley, Edinburgh Dublin Philosoph. Mag. J. Sci. **26**, 1024 (1913).
45. V. V. Medvedev, A. J. van den Boogaard, R. van der Meer, A. E. Yakshin, E. Louis, V. M. Krivtsun, and F. Bijkerk, Opt. Express **21**, 16964 (2013).
46. D. M. Miles, J. A. McCoy, R. L. McEntaffer, C. M. Eichfeld, G. Lavallee, M. Labella, W. Drawl, B. Liu, C. T. DeRoo, and T. Steiner, Astrophys. J. **869**, 95 (2018).
47. H. Mizoguchi, H. Nakarai, T. Abe, K. M. Nowak, Y. Kawasuji, H. Tanaka, Y. Watanabe, T. Hori, T. Kodama, Y. Shiraishi, T. Yanagida, G. Soumagne, T. Yamada, T. Yamazaki, S. Okazaki, and T. Saitou, Adv. Opt. Technol. **4**, 297 (2015).
48. Q. Huang, M. de Boer, J. Barreaux, D. M. Paardekooper, T. van den Boogaard, R. van de Kruijs, E. Zoethout, E. Louis, and F. Bijkerk, Proc. SPIE **9048**, 90480G (2014).
49. M. Trost, S. Schroder, A. Duparre, S. Risse, T. Feigl, U. D. Zeitner, and A. Tunnermann, Opt. Express **21**, 27852 (2013).
50. E. Spiller, AIP Conf. Proc. **75**, 124 (1981).
51. E. Spiller, Appl. Opt. **15**, 2333 (1976).
52. P. P. Naulleau,J. A. Liddle, F. Salmassi, E. H. Anderson, and E. M. Gullikson, Proc. SPIE **5347**, 9 (2003).
53. Q. Huang, V. Medvedev, R. van de Kruijs, A. Yakshin, E. Louis, and F. Bijkerk, Appl. Phys. Rev. **4**, 011104 (2017).
54. P. P. Naulleau, W. C. Sweattb, and D. A. Tichenorc, Opt. Commun. **214**, 31 (2002).
55. P. P. Naulleau, J. A. Liddle, E. H. Anderson, E. M. Gullikson, P. Mirkarimi, F. Salmassi, and E. Spiller, Opt. Commun. **229**, 109 (2004).
56. P. P. Naulleau, E. H. Anderson, E. M. Gullikson, and J. Bokor, Opt. Commun. **200**, 27 (2001).


https://doi.org/10.1017/hpl.2023.53 Published online by Cambridge University Press

57. J. A. Liddle, F. Salmassi, P. P. Naulleau, and E. M. Gullikson, J. Vac. Sci. Technol. B **21**, 2980 (2003).
58. D. L. Voronov, E. H. Anderson, E. M. Gullikson, F. Salmassi, T. Warwick, V. V. Yashchuk, and H. A. Padmore, Opt. Lett. **37**, 1628 (2012).
59. D. L. Voronov, E. M. Gullikson, F. Salmassi, T. Warwick, and H. A. Padmore, Opt. Lett. **39**, 3157 (2014).
60. Q. Huang, M. de Boer, J. Barreaux, R. van der Meer, E. Louis, and F. Bijkerk, Opt. Express **22**, 19365 (2014).
61. Q. Huang, D. M. Paardekooper, E. Zoethout, V. V. Medvedev, R. van de Kruijs, J. Bosgra, E. Louis, and F. Bijkerk, Opt. Lett. **39**, 1185 (2014).
62. T. Feigl, M. Perske, H. Pauer, T. Fiedler, U. Zeitner, R. Leitel, H.-C. Eckstein, P. Schleicher, S. Schröder, M. Trost, S. Risse, R. Steinkopf, C. Laubis, and F. Scholze, in *2016 EUVL Workshop* (2016).
63. H. Mizoguchi, in *2014 International Workshop on EUV Lithography* (2014).
64. H. Mizoguchi, K. M. Nowak, H. Nakarai, T. Abe, T. Ohta, Y. Kawasuji, H. Tanaka, Y. Watanabe, T. Hori, T. Kodama, Y. Shiraishi, T. Yanagida, T. Yamada, T. Yamazaki, S. Okazaki, and T. Saitou, J. Laser Micro. Nanoeng. **11**, 276 (2016).
65. H. Mizoguchi, H. Nakarai, T. Abe, H. Tanak, Y. Watanabe, T. Hori, Y. Shiraishi, T. Yanagida, G. Sumangne, T. Yamada, T. Saitou, N. M. Felix, and A. Lio, Proc. SPIE **11609**, 1160919 (2021).
66. H. Nakarai, T. Abe, K. M. Nowak, Y. Kawasuji, H. Tanaka, Y. Watanabe, T. Hori, T. Kodama, Y. Shiraishi, T. Yanagida, G. Soumagne, T. Yamada, T. Yamazaki, and T. Saitou, in *EUV Source Workshop* (2017).
67. K. C. Johnson, https://vixra.org/abs/1512.0295 (2018).
68. W. A. Soer, P. Gawlitza, M. M. J. W. van Herpen, M. J. J. Jak, S. Braun, P. Muys, and V. Y. Banine, Opt. Lett. **34**, 3680 (2009).
69. E. Spiller, S. L. Baker, P. B. Mirkarimi, V. Sperry, E. M. Gullikson, and D. G. Stearns, Appl. Opt. **42**, 19 (2003).
70. S. M. Zhang, "The research and characterization of cleaning methods and smoothing layer for the substrate of extreme ultraviolet multilayer," PhD. Thesis (Tongji Unversity, 2007).
71. H. J. Stock, F. Hamelmann, U. Kleineberg, D. Menke, B. Schmiedeskamp, K. Osterried, K. F. Heidemann, and U. Heinzmann, Appl. Opt. **7**, 1650 (1997).
72. F. Salmassi, P. P. Naulleau, and E. M. Gullikson, Appl. Opt. **45**, 2404 (2006).
73. F. Salmassi, C. N. Anderson, E. M. Gullikson, P. P. Naulleau, Proc. SPIE **6883**, 68830F (2008).
74. M. P. Ulmer, J. H. Dugard, D. Quispe, D. B. Buchholz, S. Stagon, Y.-W. Chung, J. Cao, K. Kritikos, N. Guerra, M. T. Stahl, R. Shiri, R. Vaidyanathan, J.-W. A. den Herder, K. Nakazawa, and S. Nikzad, Proc. SPIE **12181**, 1218131 (2022).
75. E. Louis, A. E. Yakshin, T. Tsarfati, and F. Bijkerk, Prog. Surf. Sci. **86**, 255 (2011).
76. J. C. Chen, "Comparison of ultra-precision machined surface roughness measurement methods and power spectral density characterization," PhD. Thesis (Harbin Institute of Technology, 2009).
77. P. Li, "Surface topography evaluation and error compensation based on white light interferometry," Master's Thesis (Dalian University of Technology, 2021).
78. L. Yang, X. L. Zheng, and B. Chen, Opt. Precision Eng. **19**, 2565 (2011).
79. J. Wang, L. P. Wang, C. S. Jin, and Y. Xie, China patent 104317168B (March 3, 2016).
80. I. Schuster, W. Merkel, G. Metalidis, and H. Kierey, US patent 10,503,075 B2 (December 10, 2019).
81. J. Eastman and P. Bausmeister, Opt. Commun. **12**, 418 (1974).
82. T. Feigl, M. Perske, H. Pauer, and T. Fiedler, in *2014 International Symposium on Extreme Ultraviolet Lithography* (2014).
83. L. Mazule, S. Liukaityte, R. C. Eckardt, A. Melninkaitis, O. Balachninaite, and V. Sirutkaitis, J. Phys. D: Appl. Phys. **44**, 505103 (2011).
84. J. Böhm, M. Jech, and M. Vellekoop, Tribol. Lett. **37**, 209 (2010).
85. C. Wei, "Surface quality detection technology of optical components based on regional scattering," Master's Thesis (Xi'an Technological University, 2022).
86. E. Hilpert, J. Hartung, H. von Lukowicz, T. Herffurth, and N. Heidler, Opt. Eng. **58**, 092613 (2019).
87. A. F. Herrero, H. Mentzel, V. Soltwisch, S. Jaroslawzew, C. Laubis, and F. Scholze, Proc. SPIE **10585**, 105850P (2014).
88. S. Sun, C. Jin, B. Yu, T. Guo, S. Yao, W. Deng, and C. Li, Opt. Eng. **58**, 107102 (2019).
89. F. Scholze, C. Laubis, U. Dersch, J. Pomplun, S. Burgerc, and F. Schmidt, Proc. SPIE **6617**, 66171A (2007).
90. A. E. Yakshin, I. V. Kozhevnikov, E. Zoethout, E. Louis, and F. Bijkerk, Opt. Express **18**, 6957 (2010).
91. C. Laubis, A. Barboutis, M. Biel, C. Buchholz, B. Dubrau, A. Fischer, A. Hesse, C. Stadelhoff, V. Soltwisch and F. Scholze, Proc. SPIE **8679**, 867921 (2022).
92. C. Laubis, A. Barboutis, C. Buchholz, A. Fischer, A. Haase, F. Knorr, H. Mentzel, J. Puls, A. Schönstedt, M. Sintschuk, V. Soltwisch, C. Stadelhoff, F. Scholze, Proc. SPIE **9776**, 977627 (2016).
93. S. Grantham, C. Tarrio, T. Lucatorto, M. Kriese, Y. Platonov, J. Rodriguez, and L. Jiang, Proc. SPIE **9048**, 90481I (2014).
94. S. Schröder, T. Herffurth, M. Trost, and A. Duparré, Appl. Opt. **49**, 1503 (2010).
95. S. Schröder, T. Herffurth, H. Blaschke, and A. Duparré, Appl. Opt. **50**, C164 (2011).
96. K. C. Johnson, J. Vac. Sci. Technol. B **34**, 041608 (2016).
97. A. Hassanein, V. Sizyuk, T. Sizyuk, and K. Johnson, Proc. SPIE **10583**, 1058319 (2018).
98. H. J. Wang, C. Wei, A. L. Tian, B. C. Liu, X. L. Zhu, Proc. SPIE **12073**, 120730N (2021).


https://doi.org/10.1017/hpl.2023.53 Published online by Cambridge University Press